JOURNAL OF GEOPHYSICAL RESEARCH, VOL. 106, NO. C11, PAGES 27,103–27,115, NOVEMBER 15, 2001

Mobile-bed effects in oscillatory sheet flow

C. Marjolein Dohmen-Janssen[1]
Department of Civil Engineering, Delft University of Technology, Delft, Netherlands
Department of Civil Engineering, University of Twente, Enschede, Netherlands

Wael N. Hassan and Jan S. Ribberink
Department of Civil Engineering, University of Twente, Enschede, Netherlands

Abstract. Field observations often show a considerable variation in mean grain size along the coastal profile. Under high waves in shallow water, bed ripples are washed out, and sheet flow becomes the dominant transport mode: large amounts of sand are transported in a thin layer close to the bed, i.e., the sheet flow layer. This paper focuses on grain size influences on transport processes in oscillatory sheet flow. Experiments were carried out in the Large Oscillating Water Tunnel (LOWT) of Delft Hydraulics, in which near-bed orbital velocities in combination with a net current can be simulated at full scale. Three uniform sands with different mean grain size were used. It was found that in contradiction to expressions found in literature, both the erosion depth and the sheet flow layer thickness are larger for fine sand (D_{50} = 0.13 mm) than for coarser sand ($D_{50} \geq 0.21$ mm). Measured time-averaged velocity and concentration profiles indicate that the presence of a sheet flow layer leads to an increased flow resistance and to damping of turbulence and that these effects are stronger for a thicker sheet flow layer (i.e., for fine sand). These mobile-bed effects are analyzed further by comparing the measurements with the results of a one-dimensional vertical advection-diffusion boundary layer model. Simulating the mobile-bed effects in the model by introducing an increased roughness height and a reduced turbulent eddy viscosity showed that the roughness height is of the order of the sheet flow layer thickness and that turbulence damping increases for a decreasing grain size.

1. Introduction

At the coast, sheet flow conditions occur during storms when bed shear stresses due to near-bed orbital velocities become so large (Shields parameter >0.8–1.0) that ripples are washed out and the bed becomes plane again. The sand is transported close to the bed in a thin layer with high sand concentrations, i.e., the sheet flow layer. Because of the large bed shear stresses, large amounts of sand are transported. Therefore sheet flow is an important transport regime in coastal morphodynamics, and a definite need exists for accurate predictions of sediment transport in sheet flow conditions.

Janssen et al. [1997] showed that in oscillatory sheet flow conditions the majority of the sand is transported inside the sheet flow layer. Therefore understanding of sand transport processes inside the sheet flow layer is of great importance. Two characteristic parameters for transport processes in oscillatory sheet flow are erosion depth d_c and sheet flow layer thickness δ_s. During each half wave cycle, sediment is being picked up from the bed and deposited back onto the bed. Consequently, the bed level is moving up and down during the wave cycle. The erosion depth is the distance between the top of the bed at zero velocity (still bed level) and the top of the bed at maximum velocity. The sheet flow layer is the layer where the sediment concentrations are so high that intergranular forces and sediment-flow interaction forces are important.

Both *Asano* [1992] and *Zala Flores and Sleath* [1998] derived expressions for erosion depth based on measurements in oscillatory flow. If the critical Shields parameter is neglected (which is acceptable in sheet flow conditions), the expression of *Asano* [1992] gives a linear relation between the relative erosion depth d_c/D_{50} and the maximum Shields parameter θ_w:

$$\frac{d_c}{D_{50}} = \alpha_1 \theta_w = \alpha_1 \frac{\frac{1}{2} f_w u_a^2}{(s-1) g D_{50}}. \tag{1}$$

D_{50} is the median grain diameter, f_w is the wave friction factor, u_a is the amplitude of the near-bed orbital velocity, s is the relative density ($s = \rho_s/\rho$, where ρ_s is the density of sediment and ρ is the density of water), g is the gravity acceleration, and α_1 is a constant which Asano found to be equal to 8.5. Asano assumed $f_w = 0.01$ since he noticed that the movable friction factor under oscillatory flow is not sufficiently understood. The constant value of f_w implies that according to Asano, the value of d_c does not depend on the grain diameter.

Zala Flores and Sleath [1998] found that the erosion depth does not only depend on the Shields parameter, but also on the ratio of inertial to gravity force, expressed by the parameter S, which can also be considered as a parameter representing the local flow acceleration [*Sleath*, 1994]:

$$S = \frac{\rho u_a \omega}{(\rho_s - \rho) g}. \tag{2}$$

[1]Now at Department of Civil Engineering, University of Twente, Enschede, Netherlands.

Paper number 2000JC000513.
0148-0227/01/2000JC000513$09.00

Here ω is the angular frequency ($\omega = 2\pi/T$, where T is the wave period). For high values of S ($S > 0.2$) Zala Flores and Sleath found that plug flow may occur; that is, particles start moving as a single block, and the thickness of the mobile layer shows a sudden increase. For small values of S ($S < 0.2$) the expression of Zala Flores and Sleath for the erosion depth has the same form as the one by Asano (Equation (1)), with a value of α_1 equal to 3.0. Zala Flores and Sleath used the formula of *Jonsson* [1980] to calculate the friction factor with a roughness height of the order of the grain diameter.

The difference in the proportionality constant α_1 (8.5 or 3.0) may be partly caused by different definitions of the wave friction factor. Moreover, Zala Flores and Sleath showed that for the data of Asano the value of S is >0.2. In that case, d_c/D_{50} does not only depend on the Shields parameter but also on the parameter S and may be larger than given by their equation for $S < 0.2$.

Wilson [1987] and *Sumer et al.* [1996] derived expressions for the sheet flow layer thickness δ_s based on measurements in steady flow. Their expressions are of the same form as those for d_c/D_{50}:

$$\frac{\delta_s}{D_{50}} = \alpha_2\theta. \tag{3}$$

Here δ_s/D_{50} is the relative sheet flow layer thickness, α_2 is a constant which is equal to 10.0 [*Wilson*, 1987] or 11.8 [*Sumer et al.*, 1996]. Thus, according to the expressions of *Zala Flores and Sleath* [1998], *Wilson* [1987], and *Sumer et al.* [1996], d_c and δ_s only depend on the grain diameter through the friction factor. Applying, for example, *Swart*'s [1974] formula for the wave friction factor with a roughness height equal to the grain diameter ($k_s = D_{50}$) shows that an increasing grain diameter leads to slightly increasing friction factors and thus to slightly increasing values of d_c or δ_s.

The mobility of the bed and the high sediment concentrations in the sheet flow layer affect the transport processes in several ways. Some important mobile-bed effects are the following.

1. First is hindered settling. If sediment is settling down in high concentrations, the downward flux of sediment must be compensated by an upward flux of water. This upward flow will reduce the settling velocity of the sediment particles. For example, *Richardson and Zaki* [1954] derived an expression for the settling velocity in high sediment concentrations.

2. Next is increased bed roughness. High sediment concentrations in the sheet flow layer lead to intergranular forces and sediment-flow interactions. This may lead to an increased flow resistance or an increased bed roughness. In general, the Nikuradse roughness height of a flat bed is supposed to be of the order of the grain diameter. However, in sheet flow conditions the roughness height may be 1 or 2 orders of magnitude larger. It is often found that the roughness height is of the order of the sheet flow layer thickness [e.g., *Grant and Madsen*, 1982; *Wilson*, 1989a; *Van Rijn*, 1993], which means that it depends on the Shields parameter.

On the basis of steady flow experiments, *Sumer et al.* [1996] found that the value of the roughness height also depends on whether the sediment transport is in the "suspension mode" sheet flow regime ($w_s/u_* < 0.8$–1.0) or in the "no-suspension mode" sheet flow regime ($w_s/u_* > 0.8$–1.0). Here w_s is the settling velocity, and u_* is the friction velocity. They found that in the suspension mode sheet flow regime the roughness height depends not only on the value of the Shields parameter but also on the value of w_s/u_*.

3. Last is turbulence damping. Over the (thin) sheet flow layer, sediment concentrations decrease from the maximum value at the bed to very low values at the top of the sheet flow layer. This leads to large negative vertical concentration gradients. If the sand-water mixture is considered as a continuum, the negative concentration gradient corresponds to a negative density gradient.

Density gradients introduce buoyancy forces into the flow. Negative density gradients may cause stable stratification of the flow and inhibit the turbulent transport of mass and momentum. It is known that flow stratification occurs for fine silt and mud [e.g., *Van der Ham et al.*, 1998]. The negative density gradients in the sheet flow layer may imply that turbulence damping can also occur in sheet flow conditions.

Several models exist to describe transport processes under waves. The most simple type of models are the one-dimensional vertical (1-DV) suspension-type boundary layer models [e.g., *Fredsøe et al.*, 1985; *Ribberink and Al-Salem*, 1995; *Li and Davies*, 1996]. In these models, sediment concentrations are assumed to be so low that flow velocities are not influenced by the presence of the sediment. They consist of the Navier-Stokes equation (momentum balance) to determine flow velocities and an advection-diffusion equation, derived from the mass balance of sediment, to determine sediment concentrations. *Davies et al.* [1997] presented an intercomparison of this type of models which also included the mixing length model of *Ribberink and Al-Salem* [1995], used in the present paper. They showed that the various models give very similar results despite the difference in turbulence descriptions (i.e., a mixing length model and k and k-ε models that include turbulence damping due to stratification).

Various more complex models exist that focus on specific sheet flow layer processes. Examples are the steady flow model of *Wilson* [1987], the two-layer model of *Kaczmarek* [1990], the multiple-layer model of *Bakker and Van Kesteren* [1986], the granular-fluid model for steady flow of *Hanes and Bowen* [1985], the collisional sheet flow model of *Jenkins and Hanes* [1998], and the two-phase flow models of *Asano* [1990] and *Dong and Zhang* [1999].

In order to verify and improve predictions of transport processes in sheet flow conditions, experimental data on near-bed sediment transport processes are required. However, data on sand transport in oscillatory sheet flow conditions at prototype scale are scarce. Therefore new experiments were carried out in the Large Oscillating Water Tunnel (LOWT) of Delft Hydraulics, in which near-bed orbital velocities in combination with a net current can be simulated at full scale.

The present paper presents the experimental setup and the measurements of erosion depth, sheet flow layer thickness, and time-averaged velocity and concentration profiles for three sands with different grain size. Specific attention is paid to the effect of the sheet flow layer on the flow velocity and sediment concentration in the suspension layer. To analyze these mobile-bed effects in more detail, the measurements are compared with results of the 1-DV suspension-type boundary layer model of *Ribberink and Al-Salem* [1995]. This model serves as a reference that describes suspended transport processes without taking into account the specific processes in the sheet flow layer. It is investigated whether observed differences between the model and the measurements can indeed be explained by mobile-bed effects. Thus mobile-bed effects are simulated in

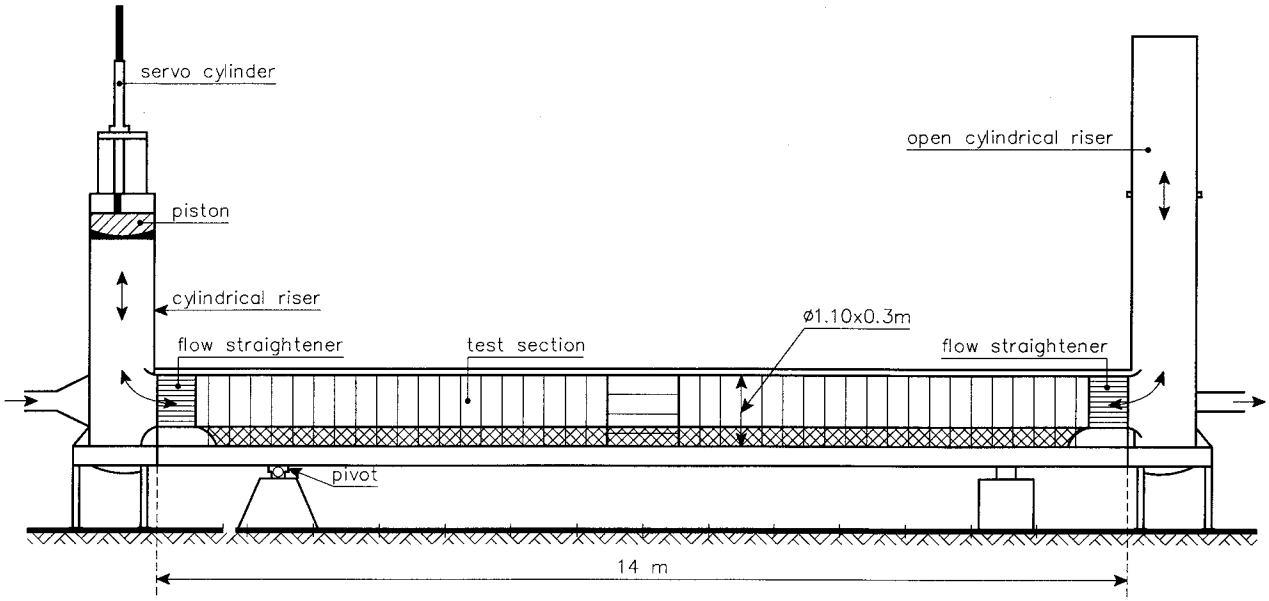

Figure 1. Outline of the Large Oscillating Water Tunnel of Delft Hydraulics.

the model by introducing an increased roughness height and a reduced turbulent eddy viscosity.

2. Experimental Setup

2.1. Large Oscillating Water Tunnel

The LOWT is a U-shaped tube, with a piston in one of the vertical cylindrical risers to generate a horizontal oscillatory flow in the test section. The other riser is open to the atmosphere. The test section (length of 12 m and width of 0.3 m) can be filled with a 0.3 m thick sand bed, leaving 0.8 m for the flow. Underneath the cylindrical risers, two sand traps are constructed to collect the sand that is eroded from the test section. Figure 1 shows the outline of the LOWT. A recirculation system allows the generation of a net current in addition to the oscillatory flow. Within the recirculation system a third sand trap is constructed in order to collect the sand that is transported by the net current.

2.2. Test Conditions and Measured Parameters

Field observations show a considerable variation in mean grain size along the coastal profile [e.g., *Terwindt*, 1962]. This means that for accurate predictions of cross-shore transport rates it is important to know the influence of the grain size on the transport process and the net transport rates. Along the Dutch North Sea coast, sand with a median grain diameter of 0.2 mm is very common. Therefore the present experiments were carried out with three narrowly-distributed sands with mean grain size D_{50} = 0.13, 0.21, and 0.32 mm. The characteristics of the sands are presented in Table 1. For reference, some tests were carried out above a fixed bed, formed by a wooden plate with the 0.21 mm sand glued on top of it.

All hydraulic conditions consisted of sinusoidal oscillatory flow plus a net current. The results presented in this paper are for a constant oscillation period T = 7.2 s. During all conditions the bed was flat, and sheet flow was the dominant transport regime. Test conditions are presented in Table 2. Part of the flow conditions were the same for all sands in order to be able to study the specific influence of the grain diameter. Table 2 includes one fixed-bed test (G4) that is relevant to the present results.

Table 2 also presents calculated values of the maximum Shields parameter θ_w, the acceleration parameter S (equation (2)), and the suspension parameter w_s/u_*. Both θ_w and u_* are based on the oscillatory velocity amplitude u_a and a wave friction factor f_w according to the formulation of *Swart* [1974] with a roughness height equal to the median grain size. For all tests the value of S is <0.2, indicating that plug flow is not expected. Values of w_s/u_* indicate that all conditions are in the suspension mode sheet flow regime ($w_s/u_* < 0.8$–1.0).

The following parameters were measured in the experiments: net transport rate, erosion depth, time-dependent velocities, and concentrations at different elevations close to the bed and sheet flow layer thickness (derived from concentration profiles). This paper presents the measured erosion depth, sheet flow layer thickness, and time-averaged velocity and con-

Table 1. Characteristics of the Three Sands Used in the Present Study[a]

	D_{10}, mm	D_{50}, mm	D_{90}, mm	σ_g, dimensionless	w_s, mm/s
Fine sand	0.10	0.13	0.18	1.30	11.4
Medium sand	0.15	0.21	0.32	1.29	26.0
Coarse sand	0.22	0.32	0.46	1.33	42.9

[a]Where D_i is diameter for which i percent of the sand (by weight) is finer, σ_g is geometric standard deviation, equal to $\frac{1}{2}[(D_{50}/D_{16}) + (D_{84}/D_{50})]$, and w_s is settling velocity of a grain with a diameter equal to D_{50}.

Table 2. Test Conditions and Measured Values of Erosion Depth

Condition	Bed	D_{50}, mm	T, s	u_a, m/s	u_m, m/s	θ_w, dimensionless	S, dimensionless	w_s/u_*, dimensionless	d_c, mm
G4	fixed	0.21	7.2	1.44	0.27	1.95	0.08	n.a.[a]	n.a.[a]
H2	mobile	0.13	7.2	0.68	0.23	0.74	0.04	0.29	0.63
H3	mobile	0.13	7.2	0.93	0.24	1.30	0.05	0.22	1.4
H4	mobile	0.13	7.2	1.09	0.25	1.74	0.06	0.19	2.0
H5	mobile	0.13	7.2	1.30	0.24	2.40	0.07	0.16	2.4
H6 (D1)	mobile	0.13	7.2	1.47	0.24	3.01	0.08	0.14	2.8
H7	mobile	0.13	7.2	0.49	0.42	0.41	0.03	0.39	0.38
H8	mobile	0.13	7.2	0.67	0.43	0.72	0.04	0.29	0.63
H9	mobile	0.13	7.2	0.94	0.43	1.33	0.05	0.22	1.6
J1	mobile	0.21	7.2	1.06	0.24	1.12	0.06	0.42	1.0
J2	mobile	0.21	7.2	1.28	0.25	1.57	0.07	0.36	1.5
E2 (D2)	mobile	0.21	7.2	1.47	0.23	2.02	0.08	0.31	2.0
J3	mobile	0.21	7.2	0.46	0.41	0.25	0.02	0.89	0.25
J4	mobile	0.21	7.2	0.65	0.41	0.46	0.04	0.66	0.5
E4	mobile	0.21	7.2	0.95	0.44	0.92	0.05	0.47	1.0
I1 (D3)	mobile	0.32	7.2	1.47	0.26	1.44	0.08	0.50	2.0
I2	mobile	0.32	7.2	1.70	0.25	1.87	0.09	0.44	2.5
I3	mobile	0.32	7.2	0.65	0.42	0.33	0.04	1.03	0.5
I4	mobile	0.32	7.2	0.92	0.42	0.62	0.05	0.76	1.0
I5	mobile	0.32	7.2	1.50	0.45	1.49	0.08	0.49	2.5

[a]Here n.a. is not applicable.

centration profiles. The results of the other measurements are given by C. M. Dohmen-Janssen et al. (Phase-lags in oscillatory sheet flow, submitted to *Coastal Engineering*, 2001) and *Dohmen-Janssen* [1999].

2.3. Measuring Techniques

The erosion depth was recorded through the glass wall, using a normal video camera. A transparent grid with millimeter scales was glued onto the glass window in the recording area. The recording area was ~50 mm × 70 mm (height × width).

A two-dimensional forward scatter laser-Doppler anemometer (LDA), developed by Delft Hydraulics [*Klopman*, 1994], was used to measure horizontal and vertical components of flow velocity, without flow disturbance. The LDA has a small sampling volume, with a height and width in flow direction of 0.22 mm and a width in cross direction of 6.5 mm. The LDA it is not capable of measuring velocities very close to the bed owing to blockage of the laser beams by sediment particles.

Therefore closer to the bed, velocities were measured using a three-dimensional acoustic Doppler velocimeter (ADV) [see *Lohrmann et al.*, 1994], which is able to measure velocities in relatively high concentrations of sediment (up to ~100 g/L). The sampling volume of the ADV is located ~0.1 m below the probe and has the shape of a (vertical) cylinder with a diameter of 6 mm and a height of ~6 mm.

A transverse suction system [*Bosman et al.*, 1987] was used to measure time-averaged concentration profiles of suspended sediment concentration. The system consists of 10 intake nozzles with an inner diameter of 3 mm, oriented transverse to the oscillatory flow. The volume of the collected sand samples was determined using calibrated tubes and then converted into sand mass.

Time-dependent suspended sediment concentrations were measured using an optical concentration meter (OPCON), designed by Delft Hydraulics [*Bosman*, 1984]. The OPCON measures volume concentration in the range of 0.005–2.0% (≈0.1–50 g/L) and is based on the extinction of infrared light. The light beam has a thickness of 2.6 mm (equal to the height of sensing volume). The distance between the optical transmitter and the receiver is 30 mm (equal to the length of sensing volume).

A conductivity concentration meter (CCM), developed by Delft Hydraulics, was used to measure concentrations in the sheet flow layer and inside the sand bed. This instrument measures high sand concentrations (≈100–1600 g/L) with a four point electroresistance method [*Ribberink and Al-Salem*, 1995]. The measured signal is proportional to the electroresistance of the sand-water mixture in a small sensing volume directly above the electrodes. The distance between the electrodes (thickness of 0.3 mm) is 0.6 mm. The horizontal length of the sensing volume is ~2 mm. The height of the sensing volume (above the ends of the electrodes) is ~1 mm. The CCM was installed into the tunnel from below, through the tunnel bottom, in order to minimize flow disturbance. For more details about the measuring techniques, see *Dohmen-Janssen* [1999].

3. Experimental Results

3.1. Erosion Depth d_c

Figure 2 shows a schematic diagram of the sand bed around flow reversal (zero velocity; left panel) and at the moment of maximum velocity (right panel). For all conditions presented in Table 2 the movement of the sand bed was recorded by video camera and used to determine the erosion depth d_c, i.e., the difference in bed level at zero and at maximum velocity. The measured values of d_c have an accuracy of about ±0.25 mm and are presented in Table 2.

Figure 3 shows measured values of d_c/D_{50} as a function of maximum Shields parameter θ_w. Here θ_w is again based on the amplitude of the oscillatory velocity u_a and *Swart*'s [1974] formula for the wave friction factor with a roughness height equal to D_{50} (see Table 2). Figure 3 shows that for each individual sand size a linear relation between d_c/D_{50} and θ_w is present. However, for a certain value of θ_w, measured values of d_c/D_{50} are clearly larger for fine sand than for medium and coarse sand.

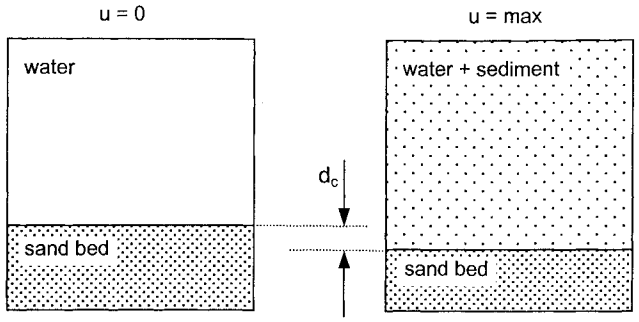

Figure 2. Schematic diagram of the sand bed around flow reversal (zero velocity; left panel) and at the moment of maximum velocity (right panel).

In other words, the data do not fall on a single line, as suggested by the expressions of *Asano* [1992] and *Zala Flores and Sleath* [1998], which are shown in Figure 3 as indications. It must be noted that the applied wave friction factor and roughness height are similar to what *Zala Flores and Sleath* [1998] used. Applying $f_w = 0.01$, as assumed by *Asano* [1992], would increase the values of θ_w for the data (by about a factor 1.2–1.7). Still, it can be concluded that measured values of d_c/D_{50} are of the same order of magnitude as the predicted values. However, in contradiction with the expressions, measured values of d_c/D_{50} for fine sand are larger than for medium and coarse sand.

The maximum Shields parameter θ_w is based on the oscillatory velocity only. If the erosion depth is related to the instantaneous velocity or shear stress, the value of d_c is expected to be higher for a higher net current velocity and a constant oscillatory velocity because of the higher maximum velocity. There are only a few data points with the same oscillatory velocity (same θ_w) and a different net current velocity. The value of d_c seems indeed to be slightly higher for a higher net current velocity. However, the difference is at most 0.5 mm, which is hardly significant. This is probably caused by the fact that the all conditions are still wave-dominated, although the current strength is significant in some cases. For more current-dominated conditions it might be more appropriate to relate values of d_c/D_{50} to a combined wave-current Shields parameter θ_{cw}.

The difference between fine sand and the two coarser sands may indicate that fine sand is in a different transport regime,

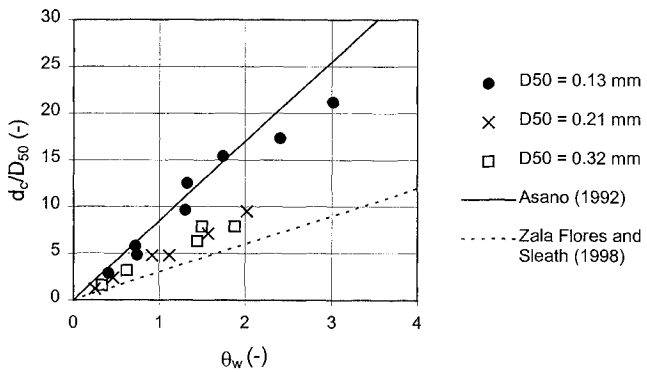

Figure 3. Nondimensional erosion depth d_c/D_{50} against Shields parameter θ_w. Measured values and expressions of *Asano* [1992] and *Zala Flores and Sleath* [1998].

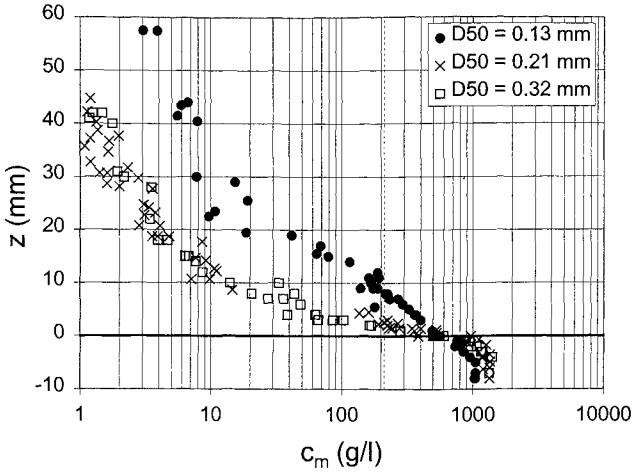

Figure 4. Time-averaged concentration profiles in the sand bed and in the lower 60 mm above the sand bed for different grain sizes.

like the bursting regime described by *King* [1991] or the plug flow regime described by *Zala Flores and Sleath* [1998] and *Sleath* [1999]. Zala Flores and Sleath found that plug flow occurs if the value of the acceleration parameter S is larger than ~0.2. However, for the present experiments the value of the parameter S is never >0.1. Moreover, the values for S for fine sand are in the same range (0.03–0.08) as those for the two coarser sands (0.02–0.09).

Straight lines can be fitted to the data of fine sand and to the data of medium and coarse sand in order to determine the proportionality coefficient α_1 between d_c/D and θ_w, observed in the measurements. The following values of α_1 are found: $\alpha_1 = 7.8$ for fine sand and $\alpha_1 = 4.5$ for medium and coarse sand, which shows that for fine sand the values of d_c/D_{50} are about a factor 1.7 larger than for medium and coarse sand. This results in the following expressions for d_c/D_{50} as a function of θ_w:

$$\frac{d_c}{D_{50}} = 7.8\theta_w \qquad D_{50} = 0.13 \text{ mm} \tag{4}$$

$$\frac{d_c}{D_{50}} = 4.5\theta_w \qquad D_{50} \geq 0.21 \text{ mm}. \tag{5}$$

3.2. Sheet Flow Layer Thickness

The sheet flow layer is defined as the layer where concentrations are so high that intergranular forces and sediment-flow interaction forces are important. Therefore the boundary between the sheet flow layer and the suspension layer is related to the magnitude of the sediment concentration. In the present study the thickness of the sheet flow layer δ_s is defined as the distance between the top of the nonmoving sand bed at maximum velocity and the level where the time-averaged concentration reaches a value of 8 vol %. For a concentration of 8 vol % the distance between particles is on average equal to the grain diameter. It can be expected that for higher concentrations, intergranular forces are important. Figure 4 shows measured time-averaged concentration profiles in the lower 60 mm above the bed for three tests with the same flow condition and three different grain sizes (H6, E2, and I1; see Table 2). For convenience these tests are renamed D1 (fine sand), D2 (medium sand), and D3 (coarse sand). The level $z = 0$ is defined

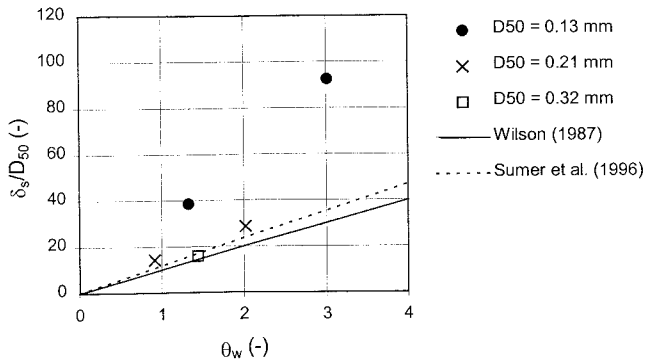

Figure 5. Nondimensional sheet flow layer thickness δ_s/D_{50} against Shields parameter θ_w. Measured values and predictions by expressions of *Wilson* [1987] and *Sumer et al.* [1996] are also shown.

at the initial bed level, which is more or less equal to the still bed level. The dashed line denotes a time-averaged concentration of 8 vol % (212 g/L). Values of sheet flow layer thickness derived from measured concentration profiles yield the following results:

H6 (D1) δ_s = 12 mm (±1 mm)

E2 (D2) δ_s = 6 mm (±1 mm)

I1 (D3) δ_s = 5 mm (±1 mm)

H9 δ_s = 5 mm (±1 mm)

E4 δ_s = 3 mm (±1 mm).

These results show that the sheet flow layer thickness δ_s for the 0.13 mm sand (D1 and H9) is about twice as large as for the medium sand (D2 and E4). For the coarse sand (D3), δ_s is about the same as for the medium sand (D2). These observations agree with the observed behavior of erosion depth.

It is important to realize that the time-averaged concentration profile might be influenced by secondary time-dependent concentration peaks due to flow reversal events [e.g., *Ribberink and Al-Salem*, 1995]. The time-dependent sediment concentration data show, indeed, that these peaks are present and that they are largest for the fine sand [*Dohmen-Janssen*, 1999]. However, they are very sharp (short duration), and it is estimated that even for fine sand, they contribute at most ~5–10% to the time-averaged sediment concentration. This would not affect the conclusion that the sediment concentration and thus the sheet flow layer thickness is much larger for fine sand than for coarser sand.

In the literature, no unique criterion exists to distinguish between sheet flow and suspension. Therefore different methods are applied to determine the sheet flow layer thickness: *Wilson* [1987] used experiments in which no suspension was present, and he took the level where the concentration becomes zero as the upper boundary of the sheet flow layer. *Sumer et al.* [1996] extrapolated the linear concentration distribution, observed near the bed, to the point of zero concentration. This gives slightly higher values of δ_s than the method applied in the present study (12–18 mm for D1, 8 mm for D2, and 7 mm for D3).

Expressions for the sheet flow layer thickness derived by Wilson and Sumer et al. are based on measurements in steady flow. For oscillatory flow, *Wilson* [1989b] suggested using the maximum Shields parameter as characteristic parameter for sheet flow layer thickness. Therefore measured values of δ_s/D_{50} are plotted against maximum Shields parameter θ_w in Figure 5 together with the expressions of Wilson and Sumer et al. Figure 5 shows that the measured sheet flow layer thickness for medium and coarse sand agrees reasonably well with the two expressions. However, the measured sheet flow layer thickness for fine sand does not at all fall on the same line as for medium and coarse sand and is much larger than predicted by the expressions.

Both the sheet flow layer thickness δ_s and the erosion depth d_c are largest for fine sand and about equal for medium and coarse sand. These two parameters are related to each other because d_c is a measure of the sediment load, i.e., the amount of sand entrained into the flow. The sediment load can be estimated as $c_b\, d_c$, where c_b is the sediment concentration in the bed. Neglecting the sediment in the suspension layer, the sediment load will be distributed over the height of the sheet flow layer, resulting in a certain concentration profile. The ratio δ_s/d_c is thus determined by the shape of the concentration distribution and it can be expected to be constant [e.g., *Sawamoto and Yamashita*, 1986].

On the basis of the measurements, values of δ_s/d_c were determined. For fine sand the average value of δ_s/d_c is ~4.5. For medium and coarse sand it is ~2.9. Apparently, the larger sediment load for fine sand (larger d_c) is distributed over a relatively larger height (4.5 d_c, rather than 2.9 d_c). On the basis of the relation between d_c and δ_s and the expressions for d_c/D_{50} derived from the present data ((4) and (5)), the following expressions for sheet flow layer thickness are derived:

$$\frac{\delta_s}{D_{50}} = 35\theta_w \qquad D_{50} = 0.13 \text{ mm} \tag{6}$$

$$\frac{\delta_s}{D_{50}} = 13\theta_w \qquad D_{50} \geq 0.21 \text{ mm}. \tag{7}$$

These expressions show that the sheet flow layer thickness for fine sand is about a factor of 2–3 larger than for medium and coarse sand.

The fact that the erosion depth, the sheet flow layer thickness, and the ratio between sheet flow layer thickness and erosion depth are all larger for fine sand (D_{50} = 0.13 mm) than for coarser sand ($D_{50} \geq 0.21$ mm) seems to indicate that fine sand is in a different transport regime, like the bursting regime described by *King* [1991] or the plug flow regime described by *Zala Flores and Sleath* [1998] and *Sleath* [1999]. However, as mentioned before, S is <0.2 (for D1, D2, and D3, $S \approx 0.08$; see Table 2), and according to Zala Flores and Sleath, plug flow should not be present.

3.3. Time-Averaged Velocity Profiles

In combined wave-current flow, wave-induced mixing in the wave boundary layer leads to a larger apparent roughness height felt by the net current above it. As mentioned in section 1, it is often suggested that the presence of a sheet flow layer also leads to increased roughness for the outer flow. This is investigated by plotting the time-averaged velocity profiles in Figure 6 for D1, D2, and D3. For D1 and D3, velocities were measured by LDA and ADV; velocities for D2 were measured only by LDA. The level z = 0 is defined at the initial (still) bed level. All velocities are normalized by their value at 100 mm

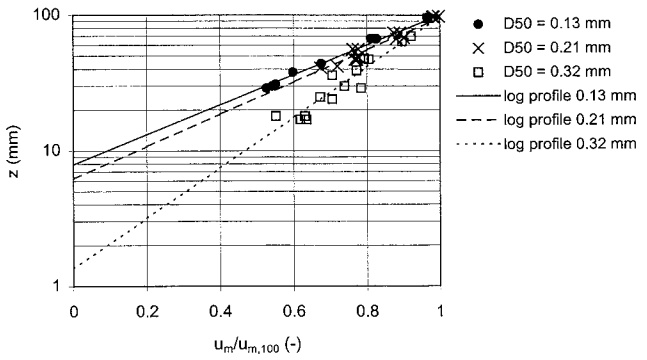

Figure 6. Nondimensional velocity profile (normalized by the time-averaged value at 100 mm above the bed, $u_{m,100}$) for fine, medium, and coarse sand.

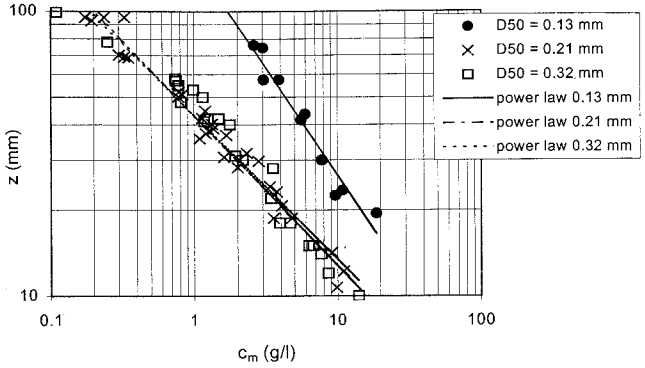

Figure 8. Time-averaged suspended sediment concentration profiles on log-log scale for different grain sizes.

above the bed. Note that according to the expression of *Sleath* [1987], the thickness of the wave boundary layer varies from ~26–34 mm for condition D1 (depending on the assumed roughness height) to ~34–44 mm for condition D3.

The time-averaged velocity seems to follow a logarithmic distribution (straight line on log-linear scale). Therefore a log profile has been fitted through the data, which is used to determine a measured apparent roughness height k_A, representing the combined effect of wave-current interaction and sediment-flow interaction. The apparent roughness height k_A is derived from the intercept of the log profile with the z axis, z_A: $k_A = 30\, z_A$. Figure 6 shows that the apparent roughness height is largest for the finest sand (0.13 mm, D1), somewhat smaller for the 0.21 mm sand (D2), and much smaller for the 0.32 mm sand (D3). The nondimensional apparent roughness height (k_A/D_{50}) varies between 100 (D3) and 1800 (D1).

For fine and medium sand these values are larger than what would be expected due to wave-current interaction only, i.e., in clear water flow above a fixed bed with a roughness height $k_s = D_{50}$. This is illustrated in Figure 7, in which measured values of k_A are plotted against median grain size D_{50} together with (1) a measured value of k_A from the fixed-bed experiment G4 and (2) values of k_A computed with the 1-DV model of *Ribberink and Al-Salem* [1995] (see section 4). The results indicate that the bed roughness, experienced by the mean flow above the wave boundary layer, is largely increased due to the presence of a mobile sand bed, at least for the two smaller grain sizes.

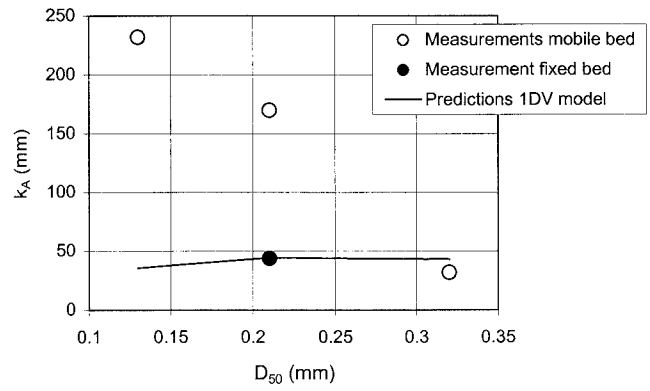

Figure 7. Measured and predicted values of apparent roughness height k_A as a function of median grain size.

3.4. Suspended Sediment Concentration Profiles

Figure 4 shows that the vertical concentration gradient in the sheet flow layer is very large. As mentioned in section 1, this may lead to damping of turbulence. The possible occurrence of turbulence damping is investigated indirectly by deriving the sediment mixing coefficient ε_{sz} from measured suspended sediment concentration profiles. *Smith* [1977] derived an expression for the time-averaged suspended sediment concentrations under waves above a plane bed (similar to the Rouse profile for steady flow), by assuming a diffusion model with a linearly increasing sediment mixing coefficient over height: $\varepsilon_{sz} = \kappa u_* z$. Here κ is the Von Karman constant, and u_* is the friction velocity. This results in a power law distribution of the time-averaged concentration (a straight line on log-log scale):

$$c_m(z) = c_a\left(\frac{z_a}{z}\right)^{\alpha}, \qquad \text{where } \alpha = \frac{w_s}{\kappa u_*} = \frac{w_s z}{\varepsilon_{sz}}, \tag{8}$$

where $c_m(z)$ is time-averaged sediment concentration at level z, c_a is reference concentration at the reference level z_a, α is concentration decay parameter, and w_s is settling velocity of the sediment. Figure 8 shows measured time-averaged suspended sediment concentration profiles for tests D1, D2, and D3. The time-averaged suspended sediment concentration is largest for fine sand and, surprisingly, about the same for the two coarser sands. Again, this is not significantly influenced by peaks in the time-dependent concentrations due to flow reversal events, which are most important for fine sand but contribute at most ~10% to the time-averaged suspended sediment concentration.

The data follow indeed straight lines on log-log scale, which indicates that a linearly increasing sediment mixing coefficient is a reasonable assumption. The value of α is determined by fitting a power law distribution to the data. These values of α are used to determine "measured" values of κu_* (using (8)). Measured values of κu_* are compared with calculated values of $\kappa u_* = \sqrt{\frac{1}{2} f_w}\, \kappa u_a$, in which the wave friction factor f_w is calculated according to *Swart*'s [1974] formula, using two different roughness heights. The results are presented in Table 3.

Applying a roughness height equal to D_{50} gives calculated values of κu_* that are almost the same for the three conditions. However, as shown in section 3.3, the roughness height is probably much larger than the median grain size. Using the measured sheet flow layer thickness as the roughness height gives somewhat higher values, which increase for decreasing

Table 3. Values of Concentration Decay Parameter α and Values of κu_* Derived From Measured Time-Averaged Suspended Sediment Concentration Profiles and Calculated Using $k_s = D_{50}$ and $k_s = \delta_{s,\text{measured}}$

			κu_*, mm/s				
				Calculated: $(\frac{1}{2}f_w)^{1/2}\kappa u_a$		Calculated: $(\frac{1}{2}f_{cw})^{1/2}\kappa u_{\max}$	
Test	D_{50}, mm	α, dimensionless	Measured	$k_s = D_{50}$	$k_s = \delta_s$	$k_s = D_{50}$	$k_s = \delta_s$
D1	0.13	1.3	8.8	32	57	36	66
D2	0.21	1.8	14	33	50	37	57
D3	0.32	1.9	23	35	49	39	55

grain size. The latter can be explained by the much larger sheet flow layer thickness for the finer sand.

Values of κu_* derived from measured suspended sediment concentration profiles are all smaller than the calculated values and decrease strongly for decreasing grain size. Smaller values of κu_* correspond to smaller values of the mixing coefficient. This might indicate that turbulence is damped due to the presence of a sheet flow layer and that turbulence damping is strongest for the finest sand, which corresponds to the thickest sheet flow layer. This may explain why the measurements show very similar concentrations for medium and coarse sand despite the smaller settling velocity for medium sand. Note that if κu_* is based on the maximum (oscillatory plus net current) velocity and a combined wave friction factor (according to the expression of *Madsen and Grant* [1976]), calculated values of κu_* are slightly higher than if only the oscillatory flow is considered (see Table 3). However, the trend is the same, and similar differences with the measured values are observed.

The present results are in line with observations of *Ribberink and Al-Salem* [1994]. They found a constant value of α for different flow conditions with the same sand (constant fall velocity), corresponding to a constant value of κu_* or mixing coefficient. The fact that the mixing coefficient did not increase for increasing velocities might indicate that turbulence damping occurred and that turbulence damping was stronger for increasing flow velocities (increasing sheet flow layer thickness).

In order to summarize the results, Figure 9 presents three characteristic measured length scales, related to mobile-bed effects, as a function of grain size for the same wave-current flow condition: (1) sheet flow layer thickness δ_s, (2) apparent roughness height k_A, and (3) suspension decay length ε_{sz}/w_s (at an arbitrary level above the sheet flow layer, i.e., $z = 0.05$ m). Figure 9 shows that all these parameters are largest for the finest sand, which indicates that the thickest sheet flow layer leads to the largest mobile-bed effects.

4. Analysis of the Data Using a 1-DV Model

In order to investigate the effects of the presence of a sheet flow layer on velocities and concentrations in the suspension layer in more detail the measurements are compared with the results of a 1-DV advection-diffusion boundary layer model, developed by *Ribberink and Al-Salem* [1995]. A short description of this model is given below.

4.1. Model Description

The model consists of the Navier-Stokes equation (momentum equation) to calculate flow velocities and an advection-diffusion equation, derived from the mass balance of sediment, to calculate suspended sediment concentrations. The equations read

$$\frac{\partial u}{\partial t} = -\frac{1}{\rho}\frac{\partial p}{\partial x} + \frac{\partial}{\partial z}\left[\nu_{tz}\frac{\partial u}{\partial z}\right] \tag{9}$$

$$\frac{\partial c_v}{\partial t} = \frac{\partial}{\partial z}\left[w_s c_v + \varepsilon_{sz}\frac{\partial c_v}{\partial z}\right]. \tag{10}$$

Here t is time, x is the distance in direction of wave propagation, z is the level above the bed, u is the horizontal flow velocity, ρ is the density of water, p is pressure, ν_{tz} is the turbulent eddy viscosity, c_v is volume concentration, w_s is the settling velocity the sediment, ρ_s is the density of sediment, and ε_{sz} is the vertical sediment diffusivity. Rather than the boundary layer flow under progressive waves, the model describes the boundary layer in a uniform horizontal oscillatory flow as present in an oscillating water tunnel. Concentrations are assumed to be so low that the flow velocity is not influenced by the presence of the sediment and that the vertical sediment velocity is equal to the settling velocity of a single sediment particle. Specific sheet flow processes, like sediment-flow interaction and grain-grain interaction, are not included.

The Boussinesq hypothesis is applied to model turbulence

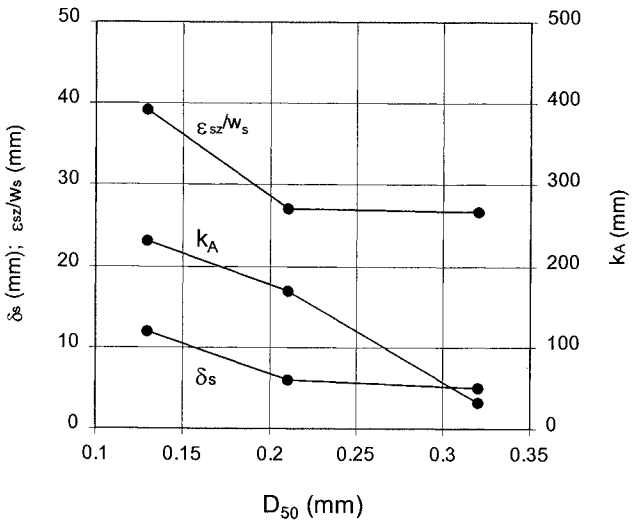

Figure 9. Characteristic measured length scales related to mobile-bed effects for the same wave-current condition as a function of grain size.

with the eddy viscosity calculated according to the mixing length theory of *Prandtl* [1932]:

$$\nu_{tz} = l_m^2 \left| \frac{\partial u}{\partial z} \right| = (\kappa z)^2 \left| \frac{\partial u}{\partial z} \right| \tag{11}$$

Here, l_m is the mixing length and κ is the Von Karman constant ($\kappa = 0.4$). Because $\partial u/\partial z$ varies with height and time, the eddy viscosity is time- and height-dependent. The sediment diffusivity is assumed to be equal to the eddy viscosity ($\varepsilon_{sz} = \nu_{tz}$ or $\beta = \varepsilon_{sz}/\nu_{tz} = 1$). Several studies have shown that the sediment diffusivity can both be larger than or smaller than the eddy viscosity (with β varying from 0.1 to 10). For example, inability of grains to follow the turbulent water motion might lead to values of ε_{sz} smaller than ν_{tz}, while centrifugal effects of eddies might lead to values of ε_{sz} larger than ν_{tz}. *Dyer and Soulsby* [1988] present an overview and notice that since the behavior of β is still poorly understood, a value of $\beta = 1$ is probably the safest choice.

The measured free stream velocity is used as the boundary condition at a level z_∞ outside the wave boundary layer. At the lower boundary the velocity is assumed to be equal to zero at $z_0 = k_s/30$, with k_s the roughness height. The roughness height is set equal to the median grain diameter ($k_s = D_{50}$) because that was found to give good agreement with the time-averaged velocity profile over a fixed bed. In addition, the horizontal pressure gradient must be known. The oscillatory component of the horizontal pressure gradient is equal to the free stream acceleration. The time-averaged component of the pressure gradient is neglected, which means that the time-averaged component of the shear stress gradient is assumed to be small compared to the acceleration term. Thus, in relation to the steady current the model assumes a constant stress layer, rather than a linearly decreasing mean stress. This is valid as long as the distance between the bed and the upper boundary of the model is small compared to the height over which the time-averaged shear stress varies (e.g., half the height of the conduit). This is generally the case if z_∞ is chosen just outside the wave boundary layer.

The advection-diffusion equation is solved by setting the vertical sediment flux equal to zero at the upper boundary. At the lower boundary, at a reference level of to $2D_{50}$, either a "reference concentration" type boundary condition or a "pick-up function" type can be imposed. In this paper a "reference concentration" type boundary condition, according to the expression of *Engelund and Fredsøe* [1976] is used in a quasi-steady way; that is, at each instant in the wave cycle, the reference concentration is calculated on the basis of the shear stress at that instant.

4.2. Comparison With Data

Figure 10 shows a comparison between measured and computed time-averaged velocity profiles (left-hand side) and time-averaged concentration profiles (right-hand side) for the three tests D1, D2, and D3. The level $z = 0$ is defined at the initial (still) bed level. The results of the 1-DV model are given by the solid line ("standard"). The dotted lines present results that will be presented in section 4.3.

Figure 10 shows that the model overestimates time-averaged velocities for all conditions. At least in the area where measurements are available, the model predicts much smaller vertical velocity gradients than observed in the measurements. This leads to strongly underestimated values of the apparent roughness height (see also Figure 7). Figure 10 shows that the deviations between the model and the measurements increase for decreasing grain size.

For fine sand (D1) and for medium sand (D2) the model overestimates time-averaged concentrations in the suspension layer. For coarse sand the model underestimates time-averaged suspended sediment concentrations. Deviations between the model results and the measurements are again largest for the finest sand (D1). Concentrations in the sheet-flow layer ($z < \sim 10$ mm) cannot be predicted correctly by the model since only suspension processes are included.

The model predicts a larger increase in concentration with decreasing grain size than observed in the measurements. This might indicate again that turbulence damping occurs and that turbulence damping is stronger for finer sand. Note that turbulence damping is not included in the model.

Strictly speaking, the differences between the model results and the measurements are not only caused by the presence of a sheet flow layer because even just bed load (rolling grains) will lead to a somewhat higher roughness. In that case the roughness height is often assumed to be $\sim 2.5\ D_{50}$. Imposing a roughness height of $2.5\ D_{50}$ in stead of D_{50} leads to negligible changes in the calculated velocity profile in the region where measurements are available, which are thus still overestimated. The concentrations will slightly increase, leading to a better agreement with the 0.32 mm data, but to a worse agreement with the concentration profiles for the 0.21 and 0.13 mm sand.

4.3. Increased Roughness and Turbulence Damping

The systematic character of the disagreement between the 1-DV model results and the measured data suggests that the discrepancies might be explained by mobile-bed effects, which are not included in the model. The measurements indicated that the sheet flow layer (1) leads to an increased resistance for the outer flow and (2) reduces the turbulence and sediment mixing in the suspension layer. In order to obtain better insight in effects of the oscillatory sheet flow layer on the outer flow (suspension layer) both processes are simulated in the model as follows: (1) The larger flow resistance or larger roughness due to the presence of the sheet flow layer is simulated by increasing the value of the imposed roughness height k_s. (2) The effect of turbulence damping is simulated by reducing the eddy viscosity ν_{tz} with a constant reduction factor β_t. Since turbulence damping will also affect the mixing of sediment, the sediment diffusivity ε_{sz} is reduced by the same amount: $\varepsilon_{sz} = \nu_{tz} = \beta_t \nu_{tz,\text{original}}$. It is examined whether predicted time-averaged velocity and concentration profiles in the suspension layer can be fitted to the data and whether the required values for the imposed roughness height k_s and the eddy viscosity reduction factor β_t are realistic and can be related to the physics involved.

It must be noted that hindered settling is not included in the model. Hindered settling will lead to larger sediment concentrations, while damping of turbulence will lead to smaller sediment concentrations. If comparisons between measurements and the improved model show that even without hindered settling a reduction in eddy viscosity is required in order to fit the sediment concentrations, it is reasonable to assume that turbulence damping occurs. Including hindered settling would lead to even larger concentrations and a stronger required reduction in eddy viscosity.

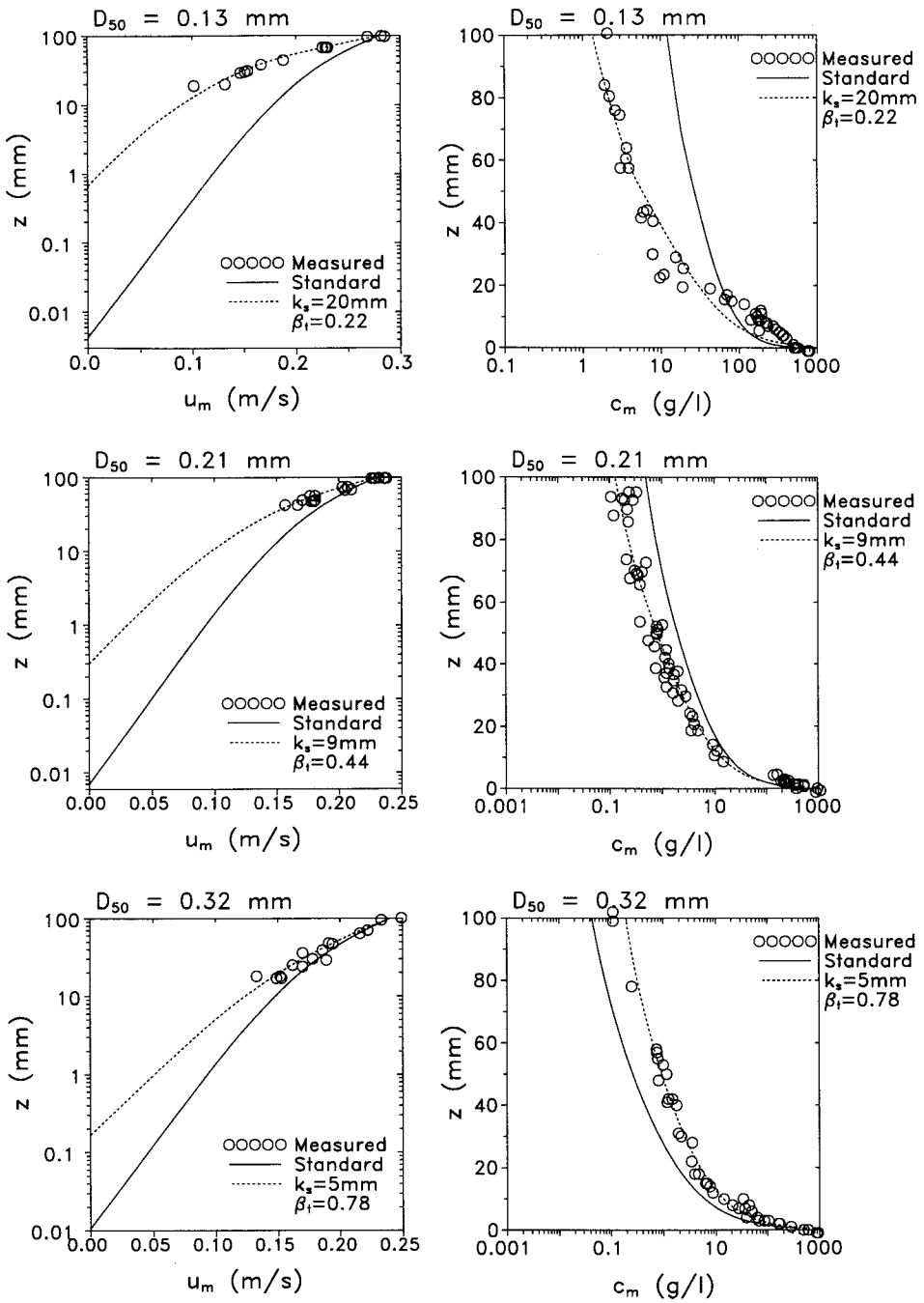

Figure 10. Measured time-averaged velocity and concentration profiles, results of the "standard" 1-DV model of *Ribberink and Al-Salem* [1995], and results of the 1-DV model with an increased roughness height (k_s) and reduced eddy viscosity (reduction coefficient β_t).

In order to show the effects of the two processes, Figure 11 first shows the effect of imposing a roughness height equal to the measured sheet flow layer thickness for condition D2. This leads to reduced time-averaged velocities, to increased velocity gradients outside the boundary layer, and to a better agreement with the measurements. However, at the same time, the time-averaged concentrations are largely increased and show worse agreement with the data.

If the eddy viscosity is then also reduced ($\beta_t = 0.49$), the reduction in time-averaged velocities and the increase in velocity gradients become stronger, and at the same time, the time-averaged concentrations are strongly reduced, leading to a good agreement with both the measured time-averaged velocity and concentration profiles above the sheet flow layer. The fact that the coefficient β_t is smaller than 1 indicates that turbulence is indeed damped due to the presence of a sheet flow layer.

The dotted lines in Figure 10 show the results of this procedure for all conditions. It turns out that for all cases a combination of roughness height and eddy viscosity reduction factor can be found, which gives reasonable agreement between the computed and measured time-averaged velocity and concentration profiles. The values of k_s and β_t required to fit the data (and the ranges over which they can vary) are pre-

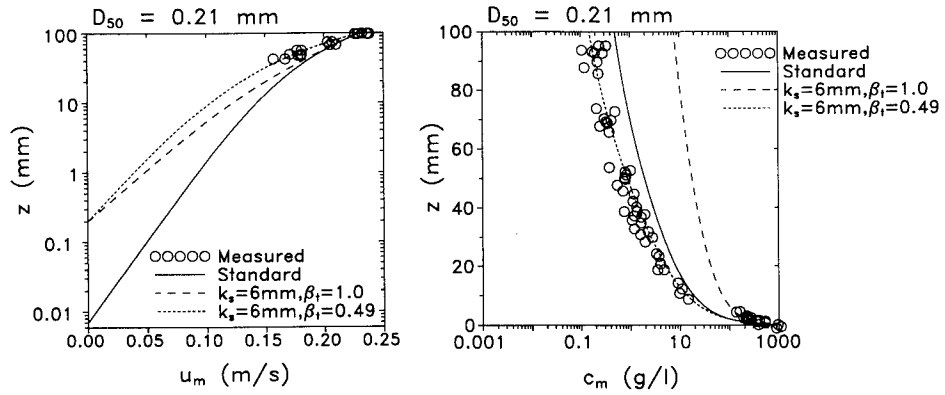

Figure 11. Measured time-averaged velocity and concentration profiles for condition D2 together with various model results: (1) standard model, (2) model with an imposed roughness height equal to the measured sheet flow layer thickness ($k_s = \delta_s$), and (3) model with $k_s = \delta_s$ and a reduced eddy viscosity.

sented in Table 4. In addition, the ratio of roughness height to measured sheet flow layer thickness (k_s/δ_s) is presented.

It was also investigated whether a good fit with the measured velocity and concentration profiles could be obtained using a combination of an increased roughness height and a reduction coefficient for the eddy diffusivity only (i.e., $\beta_t = 1$, $\beta < 1$). This does not represent turbulence damping because turbulence damping also affects the eddy viscosity, but rather represents the inability of grains to follow the turbulent water motion. In order to fit the velocity and concentration profiles, extremely large values of k_s were required (k_s/δ_s of the order of 20) and extremely small values of β were needed ($\beta < 0.1$). Moreover, the agreement between the measured and computed shape of the concentration profile was worse than for the combinations of k_s and β_t [see *Hassan*, 1996].

The results show that the required roughness height is of the order of the sheet flow layer thickness ($k_s/\delta_s = 1.0$–1.7), which means that the required roughness height is much larger than the grain size. It must be noted that in the model an increased roughness height will automatically lead to increased values of the friction velocity and therefore to increased values of the eddy viscosity and sediment mixing coefficient (by approximation $\nu_t \sim \kappa u_* z$). Therefore Table 4 also includes the parameter β_1, which represents the reduction coefficient required to compensate the (artificial) increase of the eddy viscosity due to the increased roughness. Here β_1 is defined as $u_{*D}/u_{*\delta}$, in which u_{*D} and $u_{*\delta}$ are calculated friction velocities based on the amplitude of the oscillatory velocity u_a and a wave friction factor according to the formula of *Swart* [1974] with a roughness height equal to the grain diameter or equal to the increased roughness height, presented in Table 4.

Table 4 shows that for D1 and D2 the value of β_t is clearly smaller than β_1. This means that an additional reduction in eddy viscosity is required (0.4–0.7) to fit the data, which indicates that in the measurements turbulence damping occurred for fine and medium sand. The required reduction is strongest for the finest sand, which corresponds to the fact that the sheet flow layer is thickest for the finest sand. For the coarsest sand (D3), no additional reduction is needed ($\beta_t/\beta_1 \approx 1$), which seems to indicate that for this experiment turbulent damping effects do not play a role.

The results are summarized in Figure 12, which shows the values of k_s/D_{50} and β_t/β_1, required to fit the measured time-averaged velocity and concentration profiles, as a function of grain size. Figure 12 shows that the roughness height strongly increases for decreasing grain size fine (corresponding to increasing sheet flow layer thickness) and, at the same time, the required eddy viscosity reduction coefficient decreases, indicating that turbulence damping increases.

5. Conclusions

Measurements in the Large Oscillating Water Tunnel of Delft Hydraulics showed that in oscillatory sheet flow both the erosion depth d_c and the sheet flow layer thickness δ_s are larger for fine sand ($D_{50} = 0.13$ mm) than for coarser sand ($D_{50} \geq 0.21$ mm). This is in contradiction with existing expressions, which predict values of d_c and δ_s that are almost independent of the grain size. Moreover, the ratio between sheet flow layer thickness and erosion depth is larger for fine sand than for coarser sand. These observations may indicate that fine sand is in a different transport regime.

From the measured time-averaged velocity profiles it was found that the apparent roughness is increased due to the

Table 4. Values of Roughness Height k_s and Eddy Viscosity Reduction Coefficient β_t Required to Fit the Measured Velocity and Concentration Profiles and Values of Eddy Viscosity Reduction Coefficient β_1, Required to Compensate the Increase in Eddy Viscosity Due to the Increased Roughness

Condition	δ_s, mm	k_s, mm	β_t, dimensionless	k_s/δ_s, dimensionless	β_1, dimensionless	β_t/β_1, dimensionless
D1	12	20 (16–24)	0.22 (0.24–0.20)	1.7	0.50	0.44
D2	6	9 (4–14)	0.44 (0.51–0.39)	1.5	0.61	0.72
D3	5	5 (3–7)	0.78 (0.85–0.72)	1.0	0.70	1.11

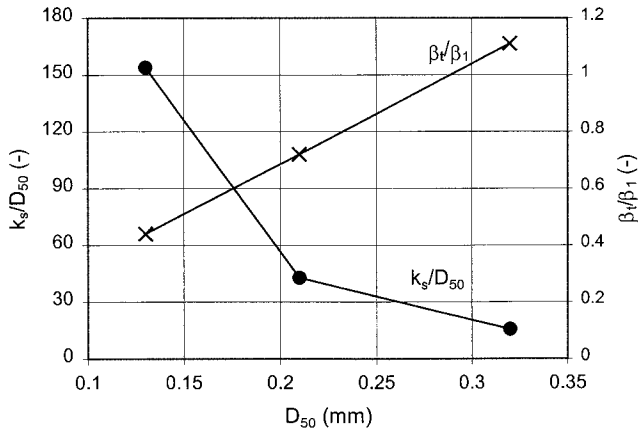

Figure 12. Values of k_s/D_{50} and β_t/β_1 required to fit the measurements, as a function of grain size.

presence of the sheet flow layer. This can be interpreted as a larger flow resistance due to intergranular forces in the sheet flow layer and interaction between flow and sediment. Measured suspended sediment concentration profiles indicated that the presence of the sheet flow layer leads to turbulence damping, which can be explained by the negative density gradients in the sheet flow layer.

Comparisons with a 1-DV advection-diffusion boundary layer model confirmed the idea that turbulence damping occurs due to the presence of a sheet flow layer. Moreover, this analysis showed that in oscillatory sheet flow the mean flow experiences a bed roughness height which is of the order of the sheet flow layer thickness. Both the roughness height and the damping of turbulence were found to increase for decreasing grain size, corresponding to an increasing sheet flow layer thickness.

Notation

c sediment concentration, g/L or kg/m^3.
c_a reference concentration at z_a, m^3/m^3.
c_m time-averaged concentration, g/l or kg/m^3.
c_v volumetric sediment concentration, m^3/m^3.
D_{50} median grain size, m.
d_c erosion depth, m.
f_w wave friction factor, dimensionless.
g gravity acceleration, m/s^2.
k_A apparent roughness height, m.
k_s bed roughness height, m.
l_m mixing length, m.
p pressure, N/m^2.
s relative density, equal to ρ_s/ρ, dimensionless.
S ratio of inertial to gravity force or acceleration parameter (equation (2)), dimensionless.
t time, s.
T wave period, s.
u horizontal velocity, m/s.
u_* friction velocity, m/s.
u_∞ horizontal free stream velocity (outside wave boundary layer), m/s.
u_a amplitude of horizontal oscillatory velocity, m/s.
u_m time-averaged horizontal velocity, m/s.
w_s settling velocity of a single sediment particle, m/s.
x distance in direction of wave propagation, m.
z level above the bed, m.
z_∞ level outside wave boundary layer where free-stream velocity is imposed, m.
z_0 $k_s/30$, m.
z_a reference level for the concentration, m.
z_A $k_A/30$, m.
α concentration decay parameter, equal to $w_s/\kappa u_*$, dimensionless.
α_1 empirical constant in expression for d_c, dimensionless.
α_2 empirical constant in expression for δ_s, dimensionless.
β_t eddy viscosity reduction coefficient, dimensionless.
δ_s sheet flow layer thickness, m.
ε_{sz} vertical sediment diffusivity, m^2/s.
ϕ sediment flux, m/s.
κ Von Karman constant (0.4).
ν_{tz} turbulent eddy viscosity, m^2/s.
θ Shields parameter, dimensionless.
θ_w maximum Shields parameter in oscillatory flow (based on u_a), dimensionless.
ρ density of water, kg/m^3.
ρ_s density of the sediment, kg/m^3.
ω angular frequency of the wave (2π/T), rad/s.

Acknowledgments. The project was funded by the Technology Foundation (STW), project DCT.2912. The authors want to thank the Dutch Ministry of Transport and Public Works (RIKZ), for the financial support to perform the experiments. Also, all the hard work during the experiments by the staff of Delft Hydraulics and by Remmelt van der Wal and Ella van der Hout, M.Sc.-students of Delft University of Technology, is greatly acknowledged.

References

Asano, T., Two-phase model on oscillatory sheet-flow, in *Proceedings of the 22nd International Conference on Coastal Engineering*, pp. 2372–2384, Am. Soc. of Civ. Eng., New York, 1990.

Asano, T., Observations of granular-fluid mixture under an oscillatory sheet flow, in *Proceedings of the 23rd International Conference on Coastal Engineering*, pp. 1896–1909, Am. Soc. of Civ. Eng., New York, 1992.

Bakker, W. T., and W. G. M. Van Kesteren, The dynamics of oscillating sheet-flow, in *Proceedings of the 20th International Conference on Coastal Engineering*, pp. 940–954, Am. Soc. of Civ. Eng., New York, 1986.

Bosman, J. J., Design and specifications of OPCON: An optical system for instantaneous concentration measurements, *Rep. R716*, part VI, Delft Hydraulics, Delft, Netherlands, 1984.

Bosman, J. J., E. T. J. M. van der Velden, and C. H. Hulsbergen, Sediment concentration measurement by transverse suction, *Coastal Eng., 11*, 353–370, 1987.

Davies, A. G., J. S. Ribberink, A. Temperville, and J. A. Zyserman, Comparisons between sediment transport models and observations made in wave and current flows above plane beds, *Coastal Eng., 31*, 163–198, 1997.

Dong, P., and K. Zhang, Two-phase flow modelling of sediment motions in oscillatory sheet flow, *Coastal Eng., 36*, 87–107, 1999.

Dohmen-Janssen, C. M., Grain size influence on sediment transport in oscillatory sheet flow, Phase-lags and mobile-bed effects, Ph.D. thesis, Delft Univ. of Technol., Delft, Netherlands, 1999.

Dyer, K. R., and R. L. Soulsby, Sand transport on the continental shelf, *Annu. Rev. Fluid Mech., 20*, 295–324, 1988.

Engelund, F., and J. Fredsøe, A sediment transport model for straight alluvial channels, *Nor. Hydrol., 7*, 293–306, 1976.

Fredsøe, J., O. H. Andersen, and S. Silberg, Distribution of suspended sediment in large waves, *J. Waterw. Port Coastal Ocean Eng., 111*, 1041–1059, 1985.

Grant, W. D., and O. S. Madsen, Movable bed roughness in unsteady oscillatory flow, *J. Geophys. Res., 87*, 469–481, 1982.

Hanes, D. M., and A. J. Bowen, A granular-fluid model for steady intense bed-load transport, *J. Geophys. Res.*, *90*, 9149–9158, 1985.

Hassan, W. N. M., Grain-size influence on the sediment transport process under waves and currents in the sheet flow regime, *Rep. H2462*, Part V, Delft Hydraulics, Delft, Netherlands, 1996.

Janssen, C. M., W. N. Hassan, R. J. van der Wal, and J. S. Ribberink, Grain-size influence on sand transport mechanisms, in *Proceedings Coastal Dynamics '97*, pp. 58–67, Am. Soc. of Civ. Eng., New York, 1997.

Jenkins, J. T., and D. M. Hanes, A sheared layer of colliding grains driven from above by a turbulent fluid, *J. Fluid Mech.*, *370*, 29–52, 1998.

Jonsson, I. G., A new approach to oscillatory rough turbulent boundary layers, *Ocean Eng.*, *7*, 109–152, 1980.

Kaczmarek, L., Mathematical model for oscillating sheet-flow, *Euromech 262, Sand transport in Rivers, Estuaries and the Sea*, edited by Soulsby and Bettess, pp. 197–202, A. A. Balkema, Brookfield, Vt., 1990.

King, D. B., Studies in oscillatory flow bedload sediment transport, Ph.D. thesis, Univ. of Calif., San Diego, La Jolla, 1991.

Klopman, G., Vertical structure of the flow due to waves and currents, *Rep. H840.30*, part II, Delft Hydraulics, Delft, Netherlands, 1994.

Li, Z., and A. G. Davies, Towards predicting sediment transport in combined wave-current flow, *J. Waterw. Port Coastal Ocean Eng.*, *122*, 157–164, 1996.

Lohrmann, A., R. Cabrera, and N. C. Kraus, Acoustic-Doppler velocimeter (ADV) for laboratory use, in *Proceedings of Symposium on Fundamentals and Advancements in Hydraulic Measurements and Experimentation*, pp. 351–365, Am. Soc. of Civ. Eng., New York, 1994.

Madsen, O. S., and W. D. Grant, Sediment transport in the coastal environment, *Rep. 209*, Ralph M. Parsons Lab. for Water Resour. and Hydrodyn., Mass. Inst. Technol., Cambridge, 1976.

Prandtl, L., Zur turbulenten Strömung in Röhren und langs Plätten, *Ergebn. Aerodyn. Versuchsanst Göttingen*, *4*, 18–29, 1932.

Ribberink, J. S., and A. A. Al-Salem, Sediment transport in oscillatory boundary layers in cases of rippled bed and sheet-flow, *J. Geophys. Res.*, *99*, 12,707–12,727, 1994.

Ribberink, J. S., and A. A. Al-Salem, Sheet flow and suspension in oscillatory boundary layers, *Coastal Eng.*, *25*, 205–225, 1995.

Richardson, Y. F., and W. N. Zaki, Sedimentation and fluidization, *Trans. Inst. Chem. Eng., Part I*, *32*, 35–53, 1954.

Sawamoto, M., and T. Yamashita, Sediment transport rate due to wave action, *J. Hydrosci. Hydraul. Eng.*, *4*, 1–15, 1986.

Sleath, J. F. A., Turbulent oscillatory flow over rough beds, *J. Fluid Mech.*, *182*, 369–409, 1987.

Sleath, J. F. A., Sediment transport in oscillatory flow, in *Sediment Transport Mechanisms in Coastal Environments and Rivers*, edited by M. Belorgey, R. D. Rajaona, and J. F. A. Sleath, World Sci., River Edge, N. J., 1994.

Sleath, J. F. A., Conditions for plug formation in oscillatory flow, *Cont. Shelf Res.*, *19*, 1643–1664, 1999.

Smith, J. D., Modelling of sediment transport on continental shelves, in *The Sea*, vol. 6, pp. 539–577, Wiley-Interscience, New York, 1977.

Sumer, B. M., A. Kozakiewicz, J. Fredsøe, and R. Deigaard, Velocity and concentration profiles in sheet-flow layer of movable bed, *J. Hydraul. Eng.*, *122*, 549–558, 1996.

Swart, D. H., Offshore sediment transport and equilibrium beach profiles, *Delft Hydraul. Lab. Publ.*, *131*, Delft Hydraulics, Delft, Netherlands, 1974.

Terwindt, J. J., Study of grain size variations at the coast of Katwijk, The Netherlands, *Note K-324*, Rijkswaterstaat, Deltadienst, Den Haag, Netherlands, 1962.

Van der Ham, R., C. Kranenburg, and J. C. Winterwerp, Turbulent vertical exchange of fine sediment in stratified tidal flows, in *Physics of Estuaries and Coastal Seas*, edited by J. Dronkers and M. Scheffers, A. A. Balkema, Brookfield, Vt., 1998.

Van Rijn, L. C., *Principles of Sediment Transport in Rivers, Estuaries and Coastal Seas*, Aqua, Amsterdam, 1993.

Wilson, K. C., Analysis of bed-load motion at high shear stress, *J. Hydraul. Eng.*, *113*, 97–103, 1987.

Wilson, K. C., Mobile bed friction at high shear stress, *J. Hydraul. Eng.*, *115*, 825–830, 1989a.

Wilson, K. C., Friction of wave-induced sheet flow, *Coastal Eng.*, *12*, 371–379, 1989b.

Zala Flores, N., and J. F. A. Sleath, Mobile layer in oscillatory sheet flow, *J. Geophys. Res.*, *103*, 12,783–12,793, 1998.

C. M. Dohmen-Janssen, W. N. Hassan, and J. S. Ribberink, Department of Civil Engineering, P. O. Box 217, University of Twente, 7500 AE Enschede, Netherlands. (c.m.dohmen-janssen@sms.utwente.nl)

(Received June 27, 2000; revised June 29, 2001;
accepted July 3, 2001.)